Controlling a Burn: Outer-Sphere Gating of Hydroxylamine Oxidation by a Distal Base in Cytochrome P460

Supporting Information

Meghan A. Smith, Sean H. Majer, Avery C. Vilbert, and Kyle M. Lancaster*

[†]Department of Chemistry and Chemical Biology, Baker Laboratory, Cornell University, Ithaca, NY 14853

Email: kml236@cornell.edu

TABLE OF CONTENTS

Experimental

General Considerations

Milli-Q water (18.2 MΩ; Millipore) was used in the preparation of all buffers and solutions. UV-visible (UV-vis) absorption spectra were obtained using a Cary 60 UV-vis spectrometer with temperature control set to 25°C. Data were fit using Igor Pro version 6.37 (WaveMetrics). For the generation of the $\{FeNO\}^6$ species, the NO-donor disodium 1-(Hydroxyl-NNO-azoxy)-L-proline (PROLI-NONOate, Cayman Chemicals) was used. The HNO-donor disodium diazen-1-ium-1,2,2-triolate (Angeli's salt, Cayman Chemicals) was used to generate the N_2O calibration curve for GC experiments. All other chemicals were purchased from VWR International.

Plasmids and Mutagenesis

Constructs for cyt P460 from *Nitrosomonas* sp. AL212 or *Nitrosomonas europaea* used in this study have been reported previously.[1, 2] Mutant variations of either cyt P460 genes were generated using site-directed mutagenesis (primers for each variant can be found in Table S1 below).

Table S1 – Site-directed mutagenesis primers; Red indicates mutagenesis sites R = reverse primer, F= forward primer

Primer Name	Sequence (5′→ 3′)
Ala131X R	GAT GCC GTT AAA CTC GCC CGG GAA ATA GCC
Ala131Glu F	GAA GCG ATG GTG AAG GAT AGC AAA CGT TAC CCG
Ala131Gln F	CAG GCG ATG GTG AAG GAT AGC AAA CGT TAC CCG
Ala131Leu F	CTG GCG ATG GTG AAG GAT AGC AAA CGT TAC CCG
Ala131Asp F	GAT GCG ATG GTG AAG GAT AGC AAA CGT TAC CCG
Glu97Ala R	CAG ACC AAT GTA ATC GCC CAT AAA ATA ACC
Glu97Ala F	GCG GCG AGC GTG AAA GAC TCT CAG CGT

Protein Expression, Purification, and Crystallization

Protein expression, purification, and crystallization for each variant was the same as for wild type (WT) *N.* sp. AL212 as previously described.[1] For the soaking experiments, 0.5 M NH_2OH or 200 μM NO generated from PROLI-NONOate were added to the cryoprotectant solution containing 30% (v/v) ethylene glycol.

Crystallographic Data Collection

X-ray diffraction measurements were carried out at beamline F1 of the Cornell High Energy Synchrotron Source (CHESS) and beamline 24-ID-E of the Advanced Photon Source (APS) Northeastern Collaborative Access Team (NE-CAT). Crystals were irradiated at 100 K using X-rays with a wavelength (λ) of 0.979 Å. X-ray diffraction data were indexed, integrated, scaled, and merged using the programs XDS[3] and CCP4.[4] An initial model was generated in Phenix[5] using the molecular replacement method and the cyt P460 structure from WT *Nitrosomonas* sp. AL212 (PDB entry 6AMG). Refinements and building to completion were then conducted using Phenix and Coot[6], respectively. PyMol[7] was used to create figures.

Steady-state Activity Assays

All assays were performed in septum-sealed cuvettes flushed with N_2 gas. Anaerobic solutions of NH_2OH were prepared and assayed by the method of Frear and Burrell[8] for determination of the stock NH_2OH concentration. Final concentrations of 50 μM 2,6-dichlorophenolindophenol (DCPIP), 6 μM phenazine methosulfate (PMS), and 1 μM cyt P460 were added to 2 mL of deoxygenated 50 mM sodium phosphate, pH 8.0. The reaction was initiated by adding an appropriate volume of the NH_2OH stock solution to the reaction mixture through the septum with a Hamilton syringe. The reaction was monitored by following the absorption of DCPIP at 605 nm. The rate of the first 10% of the total oxidant consumption was determined through linear regression. This rate was converted to the rate of oxidant consumed by using $\varepsilon_{605\ nm} = 20.6\ mM^{-1}\ cm^{-1}$.[9] Turnover frequencies (TOFs) were plotted as a function of NH_2OH concentrations. At least three trials were performed for each concentration of NH_2OH.

N_2O Assays

Production of N_2O was determined by gas chromatography using a Shimadzu GC-2010 equipped with an electron capture detector (ECD) and an Rt®-Q-Bond column (30 m, 0.25 mmID, 8 μm df). An isothermal, split method was employed with the column temperature set to 40˚C, the injection port at 200˚C, and the detector at 300˚C. Data were collected over 6 minutes.

All samples for GC analysis were prepared in 2.5 mL septum-sealed headspace vials (Chemglass Life Sciences) in an anaerobic glovebox. Turnover conditions were achieved using 1 mM DCPIP and 5 μM cyt P460 in 200 mM HEPES buffer, pH 8.0. The reactions were initiated by adding

NH_2OH to a final reaction volume of 500 µL. The headspace was sampled by a manual injection of 50 µL at a split ratio of 10. N_2O production was quantified by integrating the corresponding peak (retention time = 3.75 min). At least three trials were performed for each NH_2OH concentration.

Determination of NH_2OH and NO K_d

Cyt P460 variants were titrated with NH_2OH or NO added to septum-sealed cuvettes with a Hamilton syringe and monitored by UV-vis spectrometry. The K_d for NH_2OH was determined by following the disappearance of the shoulder feature at about 414 nm and using Equation 1:

$$A_{414\ nm} = \frac{\Delta A_{414\ nm}[NH_2OH]_0}{K_d + [NH_2OH]_0} \quad (1)$$

For the NO K_d, a similar process was repeated, but instead following the formation of the ca. 455 nm $\{FeNO\}^6$ Soret maximum. Experiments were carried out anaerobically in 50 mM sodium phosphate pH 8.0 buffer, with temperature maintained at 25 °C using a thermally jacketed cuvette holder.

Electron Paramagnetic Resonance Spectroscopy

X-band (9.40-GHz) electron paramagnetic resonance (EPR) spectra were measured on samples containing 170 µM cyt P460 variants in 50 mM sodium phosphate pH 8.0 with 25% (v/v) glycerol. Spectra were obtained using a Bruker Elexsys-II spectrometer equipped with a liquid He cryostat maintained at 10.0 K. EPR data were simulated using SpinCount.[10]

Spectroelectrochemical Potentiometric Titrations

Spectroelectrochemical titrations were performed anaerobically using a 1 mm pathlength cell (Basi) with a mesh Pt working electrode, Pt counter and Ag/AgCl reference electrode. Bulk electrolysis experiments were conducted and monitored using a WaveNow potentiostat (Pine Research) on solutions containing 200 µM cyt P460 (WT AL212, Ala131Glu, or Ala131Gln) and 20 µM methyl viologen (used as an electrochemical mediator) in 100 mM sodium phosphate pH 8.0, 100 mM NaCl. Potentials between −300 mV and −650 mV were applied in 50 mV increments from −300 mV to −500 mV, then 25 mV increments from −500 mV to −650 mV vs Ag/AgCl. Following each potential step, the solution was allowed to equilibrate for

approximately 10 mins before a UV/vis absorption spectrum was collected over the range from 200–800 nm. The resulting spectra were analyzed and fit to the linearized Nernst equation:

$$E = E^{\circ} - \frac{RT}{nF} \ln (Q) \quad (2)$$

Determination of NH_2OH and NO K_d

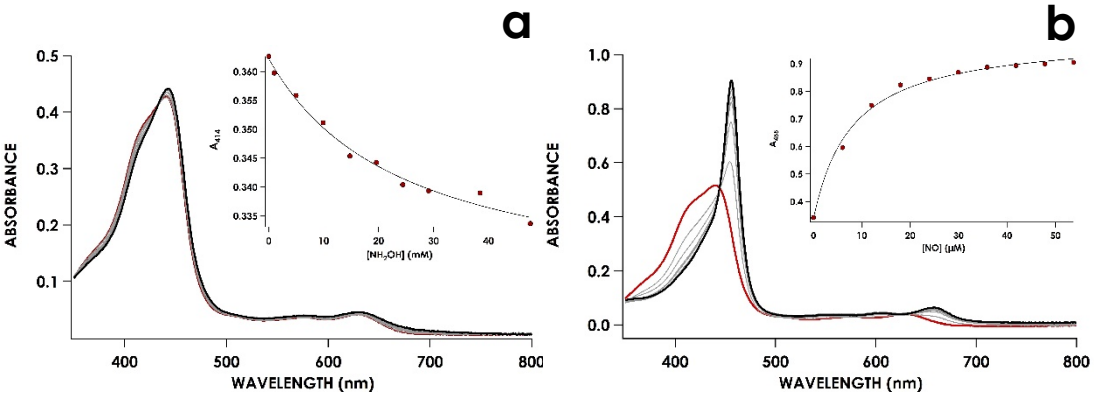

Fig. S1 Representative example of WT *N.* sp. AL212 cyt P460 titration curve with NH_2OH (a) or NO (b). Insets show the plot of hyperbolic equations to determine K_d.

Spectroelectrochemical Potentiometric Titration of Cyt P460

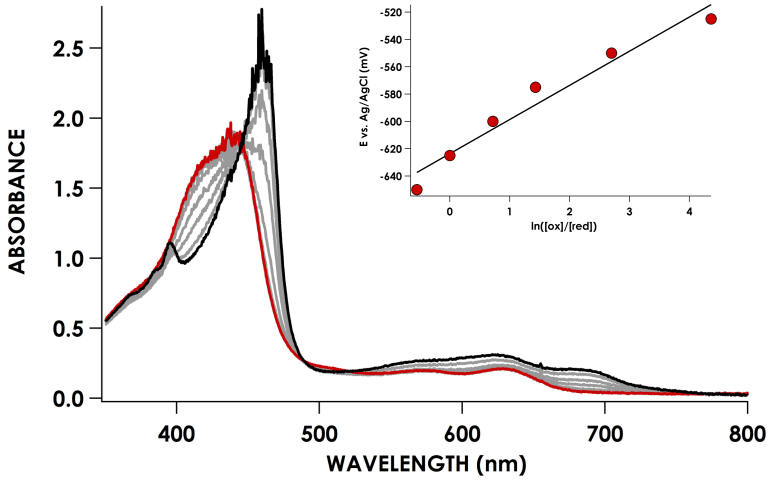

Fig. S2 UV/vis absorption spectra of WT AL212 cyt P460 at pH 8.0 as a function of applied potential. No potential was applied in the red spectrum and the following spectrums in gray are in increments of −50 mV from −300 mV to −500 mV, then −25 mV increments from −500 mV to −650 mV vs Ag/AgCl. The inset is the linearized Nernst plot of the spectroelectrochemical data. For WT *N.* sp. AL212 cyt P460 the reduction potential was determined to be −424 ± 7 mV vs. NHE, while for Ala131Glu is −428 ± 2 mV.

UV-vis Characteristics of Cyt P460 Variants

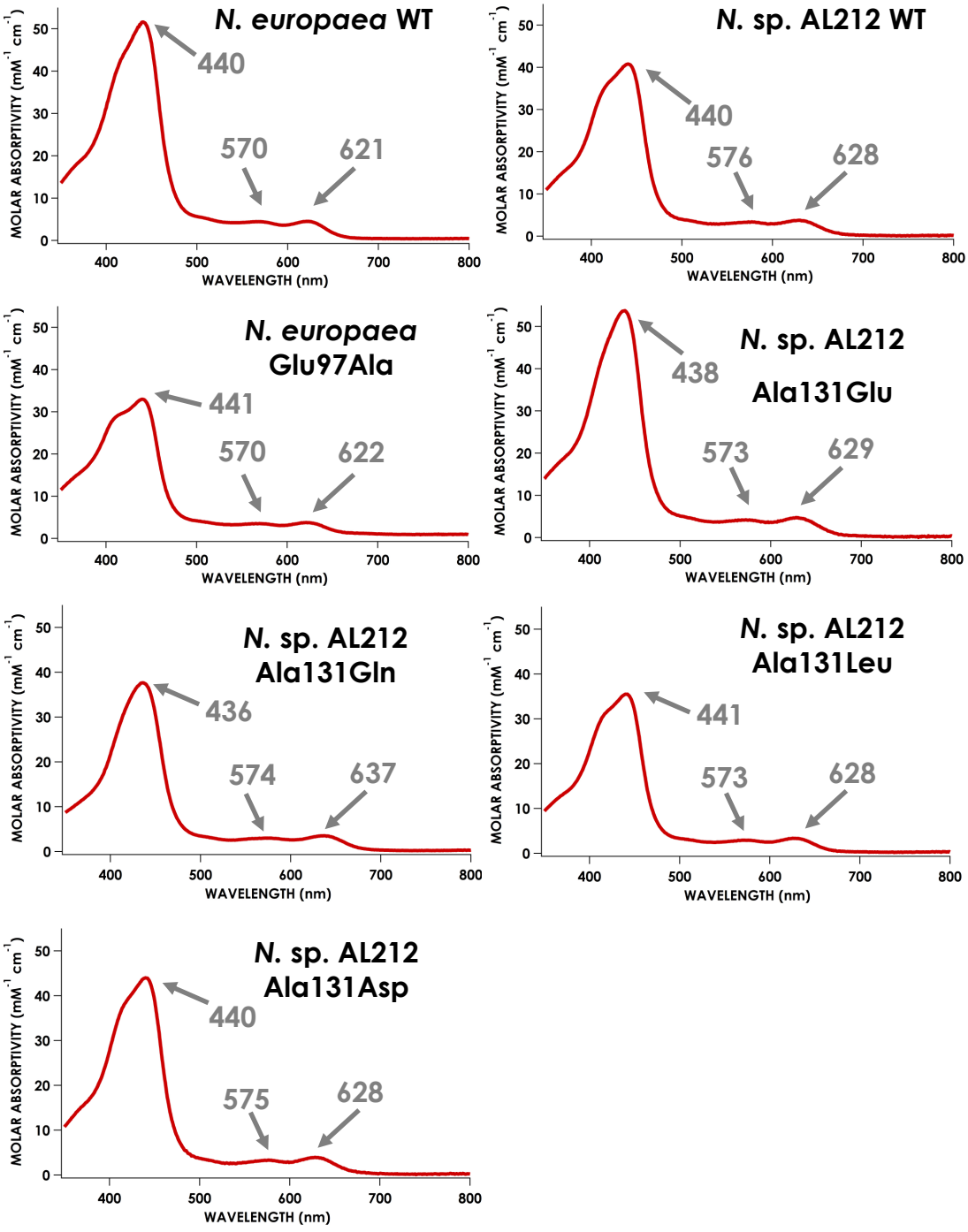

Fig. S3 UV-vis characteristics of Fe^{III} forms of cyt P460 variants.

Electron Density of Bound Substrates to Ala131Glu and Ala131Gln

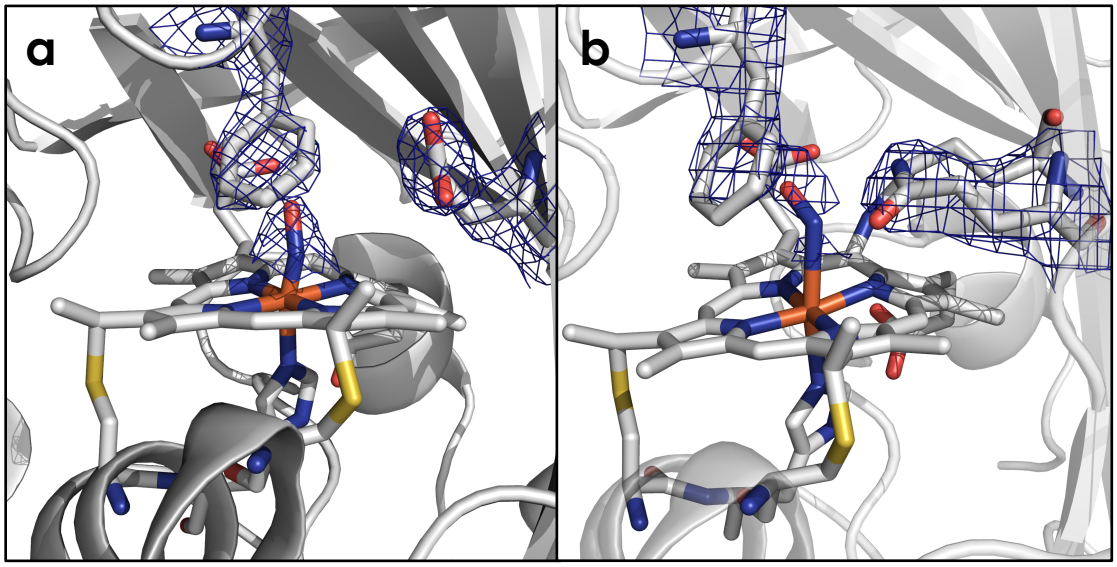

Fig. S4 $2F_o - F_c$ simulated annealing omit maps generated on final structures for Ala131Glu–NO (a) and Ala131Gln–NH_2OH (b). $2F_o - F_c$ simulated annealing omit maps represented as blue mesh, plotted at a level of 1.0 sigma.

P460 Cofactors of *N. europaea* and *N.* sp. AL212 Cyt P460s

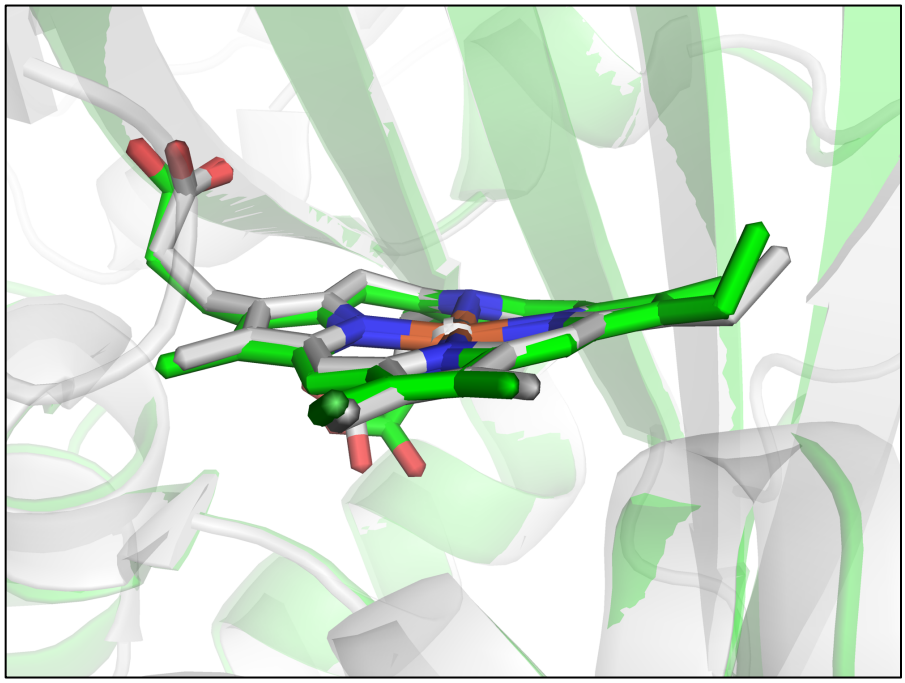

Fig. S5 Overlay of *N. euopaea* (green, PDBID: 2JE3) and *N.* sp. AL212 (grey, PDBID: 6AMG) cyt P460 cofactors.

Overlay of WT *N.* sp. AL212 and Ala131Gln Cyt P460 Structures

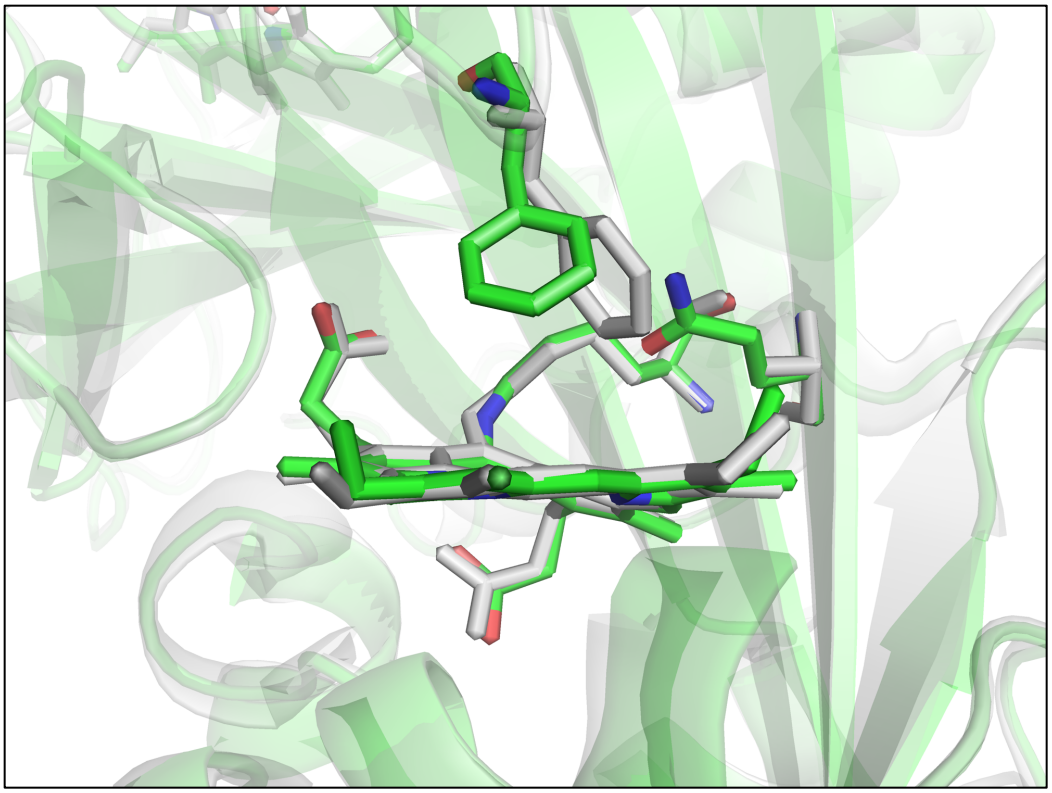

Fig. S6 Differences in the distal pockets of WT *N.* sp. AL212 (grey, PDBID: 6AMG) and Ala131Gln (green, PDBID: 6EOZ) crystal structures.

References

1. M. A. Smith and K. M. Lancaster, *Biochemistry*, 2018, **57**, 334-343.
2. J. D. Caranto, A. C. Vilbert and K. M. Lancaster, *Proc Natl Acad Sci USA*, 2016, **113**, 14704-14709.
3. W. Kabsch, *Acta Crystallogr D*, 2010, **66**, 125-132.
4. M. D. Winn, C. C. Ballard, K. D. Cowtan, E. J. Dodson, P. Emsley, P. R. Evans, R. M. Keegan, E. B. Krissinel, A. G. Leslie, A. McCoy, S. J. McNicholas, G. N. Murshudov, N. S. Pannu, E. A. Potterton, H. R. Powell, R. J. Read, A. Vagin and K. S. Wilson, *Acta Crystallogr D*, 2011, **67**, 235-242.
5. P. D. Adams, P. V. Afonine, G. Bunkoczi, V. B. Chen, I. W. Davis, N. Echols, J. J. Headd, L. W. Hung, G. J. Kapral, R. W. Grosse-Kunstleve, A. J. McCoy, N. W. Moriarty, R. Oeffner, R. J. Read, D. C. Richardson, J. S. Richardson, T. C. Terwilliger and P. H. Zwart, *Acta Crystallogr D,* 2010, **66**, 213-221.
6. P. Emsley, B. Lohkamp, W. G. Scott and K. Cowtan, *Acta Crystallogr D*, 2010, **66**, 486-501.
7. The PyMOL Molecular Graphics System, version 1.8, Schrodinger, LLC, Portland, OR, 2015.
8. D. S. Frear and R. C. Burrell, *Anal Chem*, 1955, **27**, 1664-1665.
9. G. Williamson and P. C. Engel, *Biochem J*, 1984, **218**, 521-529.
10. A. P. Golombek and M. P. Hendrich, *J Magn Reson*, 2003, **165**, 33-48.